Icarus **160**, 10–23 (2002)
doi:10.1006/icar.2002.6948

Formation of Asteroid Families by Catastrophic Disruption: Simulations with Fragmentation and Gravitational Reaccumulation

Patrick Michel and Paolo Tanga

Observatoire de la Côte d'Azur, B.P. 4229, 06304 Nice Cedex 4, France
E-mail: michel@obs-nice.fr

Willy Benz

Physikalisches Institut, University Bern, Sidlerstrasse 5, CH-3012 Bern, Switzerland

and

Derek C. Richardson

Department of Astronomy, University of Maryland, College Park Maryland 20742-2421

Received March 18, 2002; revised June 11, 2002

This paper builds on preliminary work in which numerical simulations of the collisional disruption of large asteroids (represented by the Eunomia and Koronis family parent bodies) were performed and which accounted not only for the fragmentation of the solid body through crack propagation, but also for the mutual gravitational interaction of the resulting fragments. It was found that the parent body is first completely shattered at the end of the fragmentation phase, and then subsequent gravitational reaccumulations lead to the formation of an entire family of large and small objects with dynamical properties similar to those of the parent body. In this work, we present new and improved numerical simulations in detail. As before, we use the same numerical procedure, i.e., a 3D SPH hydrocode to compute the fragmentation phase and the parallel *N*-body code `pkdgrav` to compute the subsequent gravitational reaccumulation phase. However, this reaccumulation phase is now treated more realistically by using a merging criterion based on energy and angular momentum and by allowing dissipation to occur during fragment collisions. We also extend our previous studies to the as yet unexplored intermediate impact energy regime (represented by the Flora family formation) for which the largest fragment's mass is about half that of the parent body. Finally, we examine the robustness of the results by changing various assumptions, the numerical resolution, and different numerical parameters. We find that in the lowest impact energy regime the more realistic physical approach of reaccumulation leads to results that are statistically identical to those obtained with our previous simplistic approach. Some quantitative changes arise only as the impact energy increases such that higher relative velocities are reached during fragment collisions, but they do not modify the global outcome qualitatively. As a consequence, these new simulations confirm previous main results and still lead to the conclusion that: (1) all large family members must be made of gravitationally reaccumulated fragments; (2) the original fragment size distribution and their orbital dispersion are respectively steeper and smaller than currently observed for the real families, supporting recent studies on subsequent evolution and diffusion of family members; and (3) the formation of satellites around family members is a frequent and natural outcome of collisional processes. © 2002 Elsevier Science (USA)

Key Words: **asteroids; dynamics; planetesimals; resonances; surfaces; asteroids.**

1. INTRODUCTION

In this paper, we present in detail our simulations of the collisional disruption of large asteroids in different impact energy regimes. Our aim is to establish the robustness of the gravitational reaccumulation process as a general mechanism for the formation of asteroid families (Michel *et al.* 2001). For this purpose, we have performed a number of new simulations with an improved physical treatment of the reaccumulation phase and varied various free parameters to assess the sensitivity of our results. As in Michel *et al.* (2001), we limit ourselves to solid parent bodies and leave the study of partially/totally shattered parent bodies to a forthcoming paper.

Observed asteroid families in the main asteroid belt are each composed of bodies which originally resulted from the break-up of a large parent body (e.g., Farinella *et al.* 1996). More than 20 asteroid families have been identified, corresponding to groups of small bodies well concentrated in proper orbital element space (Milani and Knežević 1990, 1992, 1994) and sharing similar spectral properties (see, e.g., Zappalà *et al.* 1995).

Interestingly, the theory of the collisional origin of asteroid families rests entirely on these similarities in dynamical and spectral properties and not on the detailed understanding of

0019-1035/02 $35.00

the collisional physics itself. Indeed, laboratory experiments on centimeter-scale targets, analytical scaling rules, or even complete numerical simulations of asteroid collisions have been so far unable to reproduce the physical and dynamical properties of asteroid families (e.g., Ryan and Melosh 1998). The extrapolation of laboratory experiments to asteroidal scales yields bodies much too weak to account for both the mass spectrum and the dynamical properties of family members. In other words, in a collision resulting in a mass distribution of fragments resembling a real family, the ejection velocities of individual fragments are much too small for them to overcome their own gravitational attraction. The parent body is merely shattered but not dispersed and therefore no family is created. Conversely, matching individual ejection velocities and deriving the necessary fragment distribution results in a mass spectrum in which no big fragment is present, contrary to most real families (e.g., Davis *et al.* 1985, Chapman *et al.* 1989).

The collisional origin of asteroid families thus implies that not only the parent body (up to several hundred kilometers in size) has been shattered by the propagation of cracks but also that the fragments generated this way typically escape from the parent and reaccumulate elsewhere in groups in order to build up the most massive family members. Such a process has already been suggested (e.g., Chapman *et al.* 1982), but the formation of many large family members by reaccumulation of smaller fragments has only been demonstrated recently (Michel *et al.* 2001). In this work, we simulated the formation of asteroid families in two extreme regimes of impact energy leading to either a small or a large mass ratio of the largest remnant to the parent body M_{lr}/M_{pb}. Our procedure used a three-dimensional SPH hydrocode to compute the fragmentation phase in the parent body due to the impact of a projectile, and a parallel N-body code to compute the subsequent gravitational interaction of the hundreds of thousands of fragments. In the present paper, we add results for the intermediate regime in which M_{lr}/M_{pb} is around 0.5.

Michel *et al.* (2001) assumed somewhat unrealistically that particles colliding during the gravitational phase always stuck perfectly and merged regardless of relative velocity and mass. Here we improve on this treatment by allowing for the dissipation of kinetic energy in such collisions and applying an energy based merging criterion (see Section 2.2 for details).

Aggregates of gravitationally bound fragments, as the ones formed in our simulations, are usually defined as *rubble-piles* in the asteroidal community, which means that they are loose aggregates of fragments held together by gravity. A detailed definition and a review of this topic are presented by Richardson *et al.* (2002). Roughly, such bodies have little to no tensile strength; i.e., they can be torn apart easily by planetary tides. Only indirect evidence for such structures exist. Indeed, the structural properties of asteroids are difficult to establish since directly measurable quantities do not distinguish between solid bodies and rubble piles. Rubble piles have been invoked to explain, for instance, the low density of some observed bodies such as 253 Mathilde whose measured density by the *NEAR* probe is 1.35 g/cm^3 (Yeomans *et al.* 1997) or the lack of fast rotators among asteroids with sizes larger than a few hundred meters (Pravec and Harris 2000). The possibility that at least the largest fragment from a collision consists of a rubble pile has been recently suggested by means of numerical simulations (Benz and Asphaug 1999). The effect of gravitational reaccumulation was then estimated by a procedure which consists of searching for gravitationally bound debris immediately following the collision (see Section 3). Decoupling the fragmentation from the subsequent gravitational reaccumulation is justified by the large time scale difference of the two processes. On one hand, cracks propagate with a velocity close to the sound speed which allows them to traverse a 100 km rocky body in a few tens of seconds. On the other hand, gravitational reaccumulation proceeds on a time scale of $\tau \geq (G\rho)^{-1/2} \approx 2200$ s (using a bulk density $\rho = 2.7$ g/cm^3). Hence, by the end of fracturing, gravity has hardly had a chance to affect the dynamics of the fragments.

In our simulations, the collisional process is carried out to late times (typically several days), during which the gravitational interactions between the fragments can eventually lead to the formation of rubble piles far from the largest remnant (Fig. 1). The new simulations also cover different collisional regimes. These regimes, from barely disruptive to highly catastrophic, can be related to three representative asteroid families (Eunomia, Flora, Koronis). The largest body in each of these families represents respectively 70%, 50%, and 4% of the mass of the parent body. In each regime, we compared the results of the simulations assuming systematic merging of colliding particles during the gravitational phase with the outcomes of simulations that allow inelastic bouncing. We also performed several simulations in which we changed different free parameters to check the sensitivity of the results and, in some cases, we also used different impact conditions to show that these lead statistically to the same outcome. In the case of Koronis, we ran a simulation in which the parent body evolved on a heliocentric orbit with parameters of the barycenter of the family and analyzed whether the presence of the Sun can influence the collisional outcome, even if the collision times scale remains rather short with respect to the orbital period.

Table I summarizes the different kinds of simulations that will be discussed. In Section 2, we recall the computational methods used to perform these simulations and explain the improvements. The procedure used to find impact conditions leading to the regime of interest is recalled in Section 3. Sections 4, 5, and 6 show the results for impact energy regimes represented by, respectively, Eunomia, Flora, and Koronis. Since several simulations have been performed for each case to check their robustness, a comparison between these simulations is also detailed in the relevant sections. Section 7 discusses the interpretation of these results in the context of the real families. Our simulations also confirm that the formation of families is generally accompanied by formation of satellites around some fragments, a topic presented in Section 8. Finally, Section 9 summarizes and discusses these results.

TABLE I
Summary of Simulation Parameters

Family	Label	Nb particles	Q (erg/g)	θ (°)	M_{lr}/M_{pb}	V_{lr} (m/s)
Eunomia	STIC	99 008	8.7×10^8	0	0.69	28
Eunomia	SPIC	99 008	8.7×10^8	0	0.69	27
Flora	I STIC	197 928	3.1×10^9	66	0.57	39
Flora	I SPIC	197 928	3.1×10^9	66	0.57	39
Flora	II STIC	197 938	7.6×10^8	14	0.59	14
Koronis	I STIC	197 931	6.8×10^9	75	0.04	76
Koronis	I SPIC	197 931	6.8×10^9	75	0.04	76
Koronis	II STIC	56 523	6.8×10^9	75	0.04	75
Koronis	IISun STIC	56 523	6.8×10^9	75	0.04	75
Koronis	III STIC	100 000	1.7×10^9	0	0.06	37
Koronis	IV STIC	100 000	3.0×10^9	42	0.05	72

Note. STIC and SPIC refer to simulations with either perfect merging of colliding particles or possible inelastic bouncing, respectively. "Nb particles" indicates the number of particles initially defining the target. Impact conditions are defined by the specific impact energy $Q =$ (Projectile kinetic energy)/(Target mass) in erg/g and the projectile's angle of incidence θ. M_{lr}/M_{pb} and V_{lr} are, respectively, the resulting mass ratio of the largest remnant to the parent body and the largest remnant ejection speed.

2. COMPUTATIONAL METHODS

2.1. Fragmentation Phase: 3D Hydrocode Simulations

Our calculations first start with an educated guess at the initial conditions needed to reproduce some observed case. The bodies are assumed to be monolithic basalt bodies with the most recent estimate of the size of the parent body of the corresponding family (Tanga *et al.* 1999). The outcome of the collision is then computed using, for the fragmentation phase, a three-dimensional smooth particle hydrodynamics (SPH) code (Benz and Asphaug 1995). This code solves in a Lagrangian framework the usual conservation equations (mass, momentum, and energy) in which the stress tensor has a nondiagonal part, the so-called deviatoric stress tensor for which the rate of change is assumed to be proportional to the strain rate (Hooke's law).

We used the so-called Tillotson equation of state for basalt (Tillotson 1962, Asphaug and Melosh 1993), which has the advantage of being computationally expedient while sophisticated enough to allow its application over a wide range of physical conditions. Plasticity is introduced by suitably modifying the stresses beyond the elastic limit using a von Mises yielding relation. For the lower tensile stresses associated with brittle failure, we used a fracture model based on the nucleation of incipient flaws whose number density is given by a Weibull distribution (Weibull 1939, Jaeger and Cook 1969).

2.2. Gravitational Phase: N-Body Simulations

The collisions considered here are energetic enough to shatter the parent bodies into fragments smaller than our numerical resolution limit. As a consequence, we are unable to derive a typical size for the boulders making up the different members of the resulting family. We can only place an upper size limit of intact fragments surviving the collision, which is typically about 2 km for a 100-km radius basaltic parent body. We do not believe that this resolution effect changes much the result of the gravitational reaccumulation phase. This is probably best evidenced by comparing the size distribution of the Koronis family members obtained using 2×10^5 and 5×10^4 particles (Fig. 4). Clearly, the differences are marginal at most.

Once the collision is over and fracture ceases, the hydrodynamical simulations are stopped and intact fragments (if any) are identified. These fragments as well as single particles and their corresponding velocity distribution are fed into an N-body code which computes the dynamical part of the evolution of the system to late time. Note that since the total mass is fixed, the extent of the reaccumulation is entirely determined by the velocity field imposed by the collisional physics upon the individual fragments.

Since we are dealing with a fairly large number of bodies that we want to follow over long periods of time, we use a parallel N-body hierarchical tree code (Richardson *et al.* 2000) to compute the dynamics. The tree component of the code provides a convenient means of consolidating forces exerted by distant particles, reducing the computational cost. The parallel component divides the work evenly among available processors, adjusting the load each time step according to the amount of work done in the previous force calculation. The code uses a straightforward second-order leapfrog scheme for the integration and computes gravity moments from tree cells to hexadecapole order. Particles are considered to be finite-sized hard spheres and collisions are identified each step using a fast neighbor-search algorithm.

We assume that fragments, regardless of their mass, have the same density ρ and always remain spherical. Thus, whenever two fragments collide and merge, the resulting single fragment is located at and given a velocity equal to the center of mass of the system, with a mass equal to the sum of the individual masses. The radius is then computed from the mass and the density, assuming spherical shape. Owing to the nature of the smoothing kernel in the SPH code, the initial conditions for the N-body code may contain some particles that overlap initially. These are merged immediately if they are less than a few tens

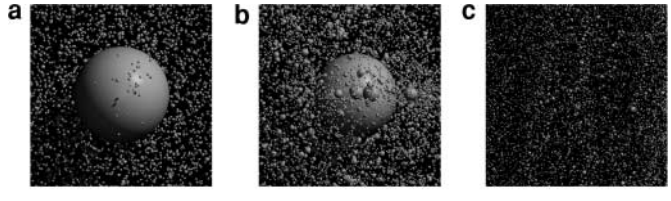

FIG. 1. Images taken from the simulations of the gravitational phase of the disruption of: (a) Eunomia, (b) Flora, (c) Koronis. These pictures show the same instant in this phase (≈84 minutes after fragmentation) and so serve to emphasize the different time scales involved in the three different impact energy regimes: the largest fragment of Eunomia is almost already formed whereas that of Flora is growing and the reaccumulation process of Koronis has barely started at this instant.

in number, otherwise the radii are reduced (keeping the mass constant) until the number of overlaps drops within this range. Some tests have been performed which indicate that the radius reduction factor does not affect the final outcome.

The simulations presented by Michel *et al.* (2001) assumed perfect sticking, which means that all colliding fragments were forced to stick regardless of their relative velocities. Here we improve our treatment of fragment collisions by using a merging criterion based on relative velocity and angular momentum. Fragments are allowed to merge only if their relative velocity is smaller than their mutual escape velocity and/or when the resulting spin of the merged fragment is smaller than the threshold value for rotational fission. Nonmerging collisions are modeled as bounces between hard spheres whose postcollision velocities are determined by the amount of dissipation taking place during the collisions. The later is determined in our simulations by the coefficient of restitution in the tangential and normal directions (see Richardson 1994 for details on this computation). Since the values of these coefficients are poorly constrained, we chose to set them arbitrarily equal to 0.5.

3. SEARCHING FOR IMPACT CONDITIONS

Since the initial conditions that lead to a given set of properties characterizing the largest member of a given family are unknown, we must proceed by trial and error until the outcome matches the required characteristics. To speed up this phase of the process, we do not integrate the system to late times using the N-body code but rather apply the iterative procedure used by Benz and Asphaug (1999) to identify the largest fragment. This procedure is adapted from techniques used in simulations of galaxy formation. The binding energy of all intact fragments with respect to the largest one, or if too small, to the one closest to the potential minimum, is first computed. This serves as a seed for nucleating the total bound mass. Unbound particles are discarded, and the center of mass position and velocity of the aggregate are computed. Using this aggregate as a new seed, the procedure is iterated until no particles are discarded. After typically 5–10 iterations, convergence is achieved and a friends-of-friends algorithm is finally used to check that fragment members of this gravitationally bound aggregate are also spatially close. Dynamical parameters such as mass, position, and velocity are also determined for this gravitationally bound aggregate. Except in the case where the largest fragment represents typically less than 10% of the parent body's mass, this procedure has been quite successful at predicting the actual characteristics of the largest remnant.

4. SIMULATIONS OF COLLISIONS IN THREE DIFFERENT REGIMES OF IMPACT ENERGY

4.1. Barely Disruptive Event: Formation of Eunomia-like Family

Our first aim was to create a family with a fairly large mass ratio M_{lr}/M_{pb} of largest remnant to parent body. A good example is the Eunomia family (Michel *et al.* 2001). The list of family members is thought to be complete for bodies with diameter larger than 11 km (the *completeness limit diameter* for this family); there are 110 Eunomia members larger than this value. However, some of these identified family members may actually be interlopers, i.e., asteroids classified as members using the standard identification techniques but not belonging to the set of fragments originating from the parent body (Migliorini *et al.* 1995). In particular, the second and third largest members are certainly interlopers, since they display featureless spectra similar to C-type asteroids, in contrast with the other members, which have been characterized as S-type (Lazzaro *et al.* 2001).

The estimated diameter of the parent body is 284 km (Tanga *et al.* 1999) and $M_{lr}/M_{pb} = 0.72$. It has thus been defined as a *partially disrupted* family (Marzari *et al.* 1999).

Results of the simulation with perfect sticking of colliding particles during the gravitational phase have already been presented (Michel *et al.* 2001). Here we present new simulations including inelastic bouncing between colliding particles during the gravitational phase. For the fragmentation phase, SPH simulations are those of Michel *et al.* (2001). In these simulations, a 284 km-sized solid target represented by $\sim 10^5$ SPH particles was broken up. Since spectral properties of Eunomia members have features of the S taxonomic type, the bulk density of the particles was assumed to be 2.7 g/cm^3, which matches the bulk density of observed S-type asteroids such as Ida (Belton *et al.* 1995) or Eros (Thomas *et al.* 2000). It is not certain that the grain density is actually equal to the bulk density for such asteroids, but since the size of the parent body is fixed, matching the bulk density implies at least the same mass for the parent body. Moreover, the choice of material for which the equation of state and fracture parameters are known is limited, and the values adopted here correspond to basalt. From the particle masses and their assumed spherical shape, a particle radius of $\approx$3.07 km is estimated. A mass ratio close to the real one ($M_{lr}/M_{pb} = 0.70$) was then produced by a "head on" collision of a projectile 48 km in diameter at 6 km/s. This corresponds to a specific impact energy $Q = E/M_{pb} = 8.7 \times 10^8$ erg/g, where E is the kinetic energy of the projectile and M_{pb} is the parent body mass. One important result is that these impact conditions completely shatter the target down to the SPH resolution limit at the end of the fragmentation phase, so that the number of fragments equals the number of initial SPH particles. However, the subsequent gravitational phase leads to the formation of a largest remnant with the expected mass as a result of gravitational reaccumulation of smaller particles. The outcome of the full process is then a mass spectrum of well-dispersed large and small fragments, in agreement with the definition of an asteroid family (Michel *et al.* 2001). In this first simulation during which colliding particles systematically merged (hereafter referred to as a STIC for *Simulation with Totally Inelastic Collisions*), the integration step size was equal to 5 s. We checked that even using 10 times this value, identical results are obtained. However, to be conservative, we will keep 5 s as a step size in all our simulations.

In order to check whether the assumption of perfect merging is not too simplistic even in a low collisional regime, we used the same starting conditions at the end of the fragmentation phase to perform several N-body simulations in which we included the possibility of particle bouncing (hereafter SPIC for *Simulation with Partially Inelastic Collisions*). The remaining particles either produce other smaller rubble piles, well separated from the largest, or simply escape the system as individual particles. Individual particles represent 27% of the parent body mass at the end of the simulation, which is similar to the 26% obtained with STIC. This shows that only a few small particles experience high velocity collisions. Thus, this improved simulation confirms the results of Michel *et al.* (2001) and shows that gravitational reaccumulation takes place and is at the origin of the formation not only of the largest remnant but also of the other large fragments with size above the simulation resolution. The outcome is finally a size distribution of fragments, which, as Fig. 2 (top) shows, almost exactly matches the one obtained with STIC. The largest remnant contains about 69% of the parent body's mass. The next two largest fragments of the distribution have diameters equal to respectively 34.5 km and 12.1 km, again of the same order as those obtained by STIC (35.04 km and 12.3 km). They are also identical to the estimated values for the real Eunomia members (32.4 km and 14.3 km), if we neglect the two bigger members identified as interlopers from their spectral properties (Lazzaro *et al.* 2001). Interpretations of these results when compared to the real family are discussed later (Section 7). The final configuration was measured 5.8 days after impact, well beyond the time (roughly 1.7 days after impact) when there were no further statistically significant changes in the size and ejection velocities.

Concerning the ejection velocities with respect to the parent body's center of mass (Fig. 5), for the 1064 fragments of diameter larger than the mimimum size constrained by the resolution, the maximum speed is 0.725 km/s, and as Table II shows, SPIC and STIC result in statistically similar fragment ejection velocities. Thus, in impact energy regimes leading to values of M_{lr}/M_{pb} well above the so-called critical value of 0.5, the details of the reaccumulation process do not have major statistical consequences on the collisional outcome.

4.2. *Intermediate Regime: Formation of Flora-like Family*

In this section, we study the intermediate regime which corresponds to M_{lr}/M_{pb} close to 0.5. An interesting example is the Flora family, which is characterized by a parent body of diameter 164 km (Tanga *et al.* 1999) and $M_{lr}/M_{pb} = 0.57$. We used 2×10^5 SPH particles to define the parent body. The minimal radius of the particles is thus $\approx$1.407 km.

For our first Flora simulation, we used a projectile 48 km in diameter impacting at 5 km/s with an angle of incidence of 66°, corresponding to $Q = 3.1 \times 10^9$ erg/g. According to the iterative procedure, this should lead to $M_{lr}/M_{pb} = 0.56$ and a largest remnant velocity close to 0.039 km/s, of the same order of the value estimated for the real one (Cellino *et al.* 1999). The

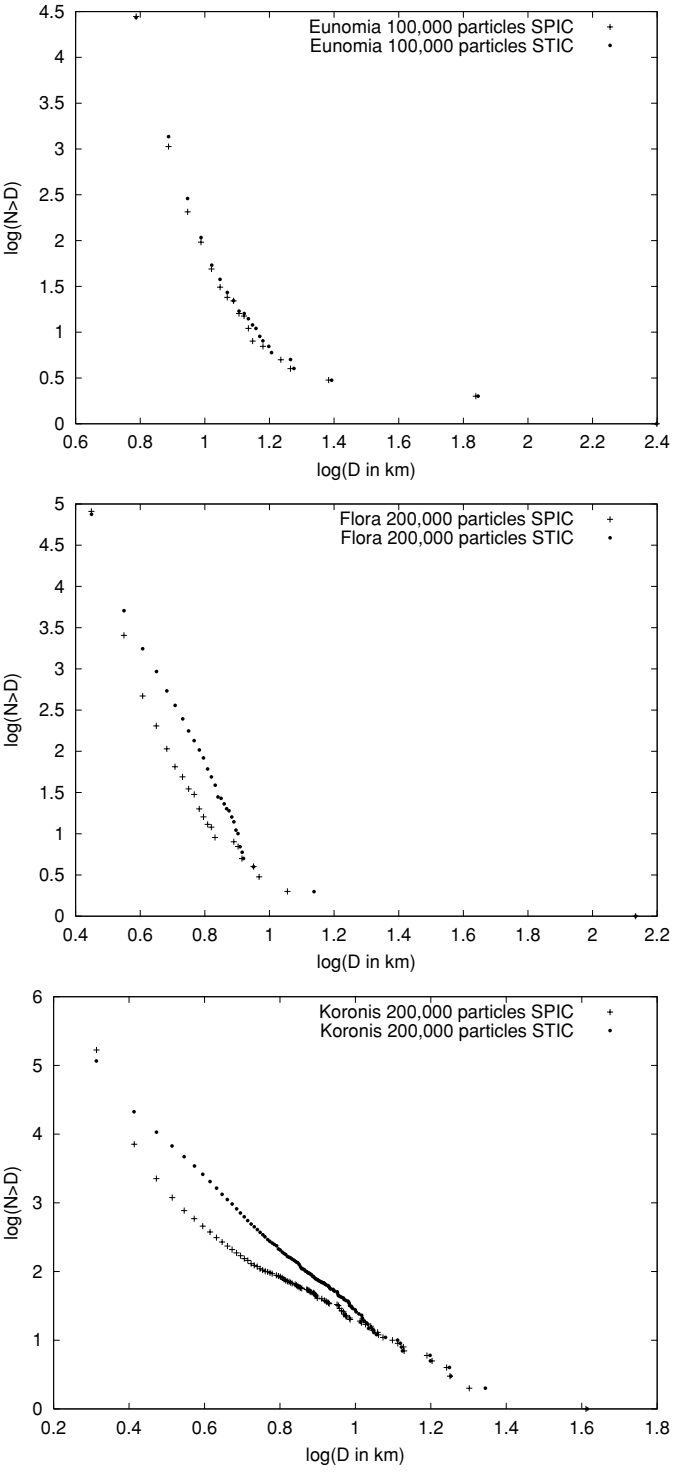

FIG. 2. Cumulative diameter distributions (in km) of the fragments resulting from the three simulations of family formation in a log–log plot: Eunomia (top), Flora (middle) and Koronis (bottom); STIC indicates simulations with perfect merging of colliding particles during the gravitational phase, whereas SPIC means that particle bouncing can occur according to fixed criteria (see text for details). The names at the top of the plots correspond to the real family names; i.e., these simulations were performed using a target with diameter and bulk density corresponding to the parent body of these families. The number of particles used to define the target is also indicated on the plots.

TABLE II

Comparison of Collisional Outcomes from Simulations Using Different Parameters (see Table I for the Definitions of Family Labels)

Family	M_{lr}/M_{pb}	α	Nb $R > R_{\min}$	$\langle V_{ej} \rangle$ (m/s)
Eunomia Real	0.70	-4.40 ± 0.42		
Eunomia STIC	0.69	-4.90 ± 0.16	1343	91 ± 37
Eunomia SPIC	0.69	-4.90 ± 0.16	1064	87 ± 38
Flora Real	0.57	-2.85 ± 0.17		
Flora I STIC	0.57	-6.63 ± 0.21	5012	87 ± 38
Flora I SPIC	0.57	-5.58 ± 0.16	2552	85 ± 42
Flora II STIC	0.59	-7.99 ± 0.25	4216	98 ± 36
Koronis Real	0.04	-2.55 ± 0.34		
Koronis I STIC	0.04	-4.56 ± 0.02	21199	128 ± 44
Koronis I SPIC	0.04	-3.20 ± 0.02	7116	92 ± 36
Koronis II STIC	0.04		5252	117 ± 44

Note. The column α gives the values of the exponent of the power law fitting the cumulative size distribution of fragments in our simulations. For the real families, these have been estimated by Tanga *et al.* (1999). The power law is defined by $N(>D) = D^{\alpha}$, where $N(>D)$ is the cumulative number of fragments with size greater than D. "Nb $R > R_{\min}$" is the number of fragments which have suffered at least one reaccumulation and $\langle V_{ej} \rangle$ (m/s) is the mean ejection speed of those fragments.

SPH simulation resulted again in a completely fragmented parent body. The gravitational interaction of the 2×10^5 fragments computed by STIC leads to $M_{lr}/M_{pb} = 0.57$ and a size spectrum composed of other large fragments with diameters ranging from 15 km down to the resolution limit as a result of gravitational reaccumulation (see Fig. 2, middle). Note that several asteroids with size greater than our 15-km second-largest fragment have been identified as members of the real Flora family. However, the characterization of the Flora family itself is subject to many uncertainties, which will be discussed in Section 7.

To check whether different impact conditions leading to the same value of M_{lr}/M_{pb} could produce a second-largest fragment with a greater diameter, we performed another STIC simulation with the same target (2×10^5 particles), but a projectile 30 km in diameter impacting at 5 km/s with an angle of incidence of 14°. The specific impact energy $Q = 7.6 \times 10^8$ erg/g is lower than the previous case, but the iterative procedure gives a similar value of M_{lr}/M_{pb}. This is consistent with previous studies, which have shown that an impact at low angle of incidence requires a lower impact energy to achieve the same degree of fragmentation as an impact at higher angle of incidence and higher impact energy (Benz and Asphaug 1999). From the N-body STIC simulation, we obtain $M_{lr}/M_{pb} = 0.59$, and a smaller velocity of the largest remnant (0.014 km/s). A second-largest fragment as small as the previous one is again obtained.

Figure 3 shows the size distribution of the fragments produced by both simulations, 11.3 days after the impact, when no significant evolution is observed anymore. As one can see, the first STIC produces more large fragments than the second one, but both distributions are very steep, starting from the third-largest fragment. Thus, qualitatively, the two impact conditions lead to the same outcome: a very steep size distribution in which the largest remnant remains well separated from the other large fragments. Note however that using a rubble pile and/or a non-spherical parent body may not lead to this conclusion and this will need further investigation.

Concerning ejection velocities, the second STIC results in a slightly larger mean value (Table II), while the largest remnant has a much smaller velocity than in the first STIC simulation.

We then ran another simulation using the first impact conditions and including the possibility of particle bouncing during the gravitational phase. This simulation (SPIC) was again stopped well after any significant changes were observed, 5.8 days after impact. It produced similar results to the STIC case. In particular, it led to $M_{lr}/M_{pb} = 0.57$ with a largest remnant velocity of 0.039 km/s. However, in this regime, more frequent collisions at high velocities occur between particles. Consequently, some differences in the size distributions of the two simulations can be noted. In particular, fewer large fragments are produced in SPIC and 2,552 fragments have a radius larger than the resolution; i.e., about half the number of those produced by STIC. Also, SPIC produces second- and third-largest fragments detached from the main distribution, unlike STIC. Statistically however, both size distributions are characterized by a very steep slope (see Fig. 2, middle) and ejection velocities are of the same order (Table II). Therefore, in the intermediate regime, the more simplistic simulation (STIC) gives the same global outcome properties as the more realistic SPIC one, even though the latter prevents many mergers from occurring due to high-speed collisions.

4.3. Highly Catastrophic Break-up: Formation of Koronis-like Family

Our last goal was to create a family with a small M_{lr}/M_{pb}, such as the Koronis family, for which the completeness limit

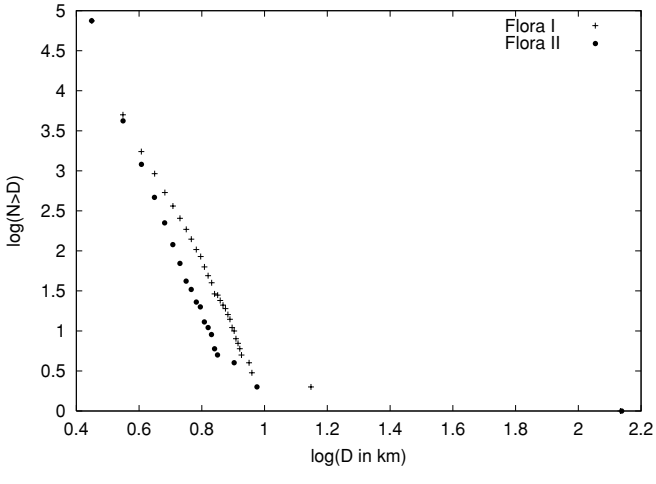

FIG. 3. Cumulative diameter distributions (in km) of the fragments resulting from the two STIC of the Flora family formation in a log–log plot. In Flora I, a projectile 48 km in diameter impacts the 164 km-size target at 5 km/s with an angle of incidence of 66°, whereas in Flora II, a projectile 30 km in diameter impacts with the same velocity but at an angle of incidence of 14°.

diameter is 13 km, above which 55 members are identified. The most recent estimate of the parent body diameter is 119 km (Tanga *et al.* 1999). For this family, $M_{lr}/M_{pb} = 0.04$, which indicates that it must have been created through a highly catastrophic event. We performed several SPH simulations using 2×10^5 SPH particles (corresponding to spherical particles of 1.029 km in radius). The impact conditions were characterized by a projectile 60 km in diameter colliding at 3.25 km/s with an angle of incidence of 75°; i.e., $Q = 6.8 \times 10^9$ erg/g. As for the previous cases, the fragmentation phase resulted in a completely shattered parent body.

The outcome of the gravitational phase using STIC was presented in Michel *et al.* (2001). Before making more realistic simulations, we performed two other STIC starting from the same impact conditions. They both used 4 times fewer SPH particles than the first one (i.e., 5×10^4 particles instead of 2×10^5), and one was performed with the parent body placed in orbit around the Sun. For the latter, we used the orbital elements of the barycenter of the real family (semi-major axis $a_b = 2.876$ AU, eccentricity $e_b = 0.048$, and inclination $I_b = 2.1°$). These two simulations were designed to check the resolution sensitivity and to see whether the presence of the Sun has an influence on the collisional outcome. Indeed, the evolution time scale in the catastrophic regime can be much longer than in impact energy regimes of lower energy, since many reaccumulations take place via mutual perturbations well after the fragments have spread out on their ejection trajectories. Consequently, the stochasticity of the process is stronger than in less energetic regimes, and greater differences can be expected between simulations which differ by changes in parameters such as the resolution. Moreover, in such a case, it becomes interesting to see whether the presence of the Sun has an effect within the time scale required to end the collisional reaccumulation process.

Figure 4 shows that the size distributions of the fragments from the simulations with 5×10^4 particles either on a heliocentric orbit or in the target's frame are almost identical. Moreover, both give similar results as the run with 4 times more particles, showing that the choice of 2×10^5 particles to define the target is rather conservative. Interestingly, the impact conditions of these simulations were all expected by the iterative procedure to result in $M_{lr}/M_{pb} = 0.08$. The accuracy of this procedure thus decreases for higher energy collisional regimes, in which reaccumulations take place at later times. In that case, the final bound particles cannot be accurately identified immediately at the end of the SPH fragmentation phase. As shown in Table II, the ejection velocities are in this case much higher than those achieved by the Eunomia fragments, which is consistent with the collisional regime of Koronis. Identical statistical results are found with the two chosen resolutions.

We next used the endstate of an SPH simulation with 2×10^5 particles to perform a simulation with inelastic bouncing allowed (SPIC) during the gravitational phase. SPIC results in a fragment size distribution, which begins to differ with that obtained by STIC at sizes smaller than ≈10 km (Fig. 2, bottom), the slope

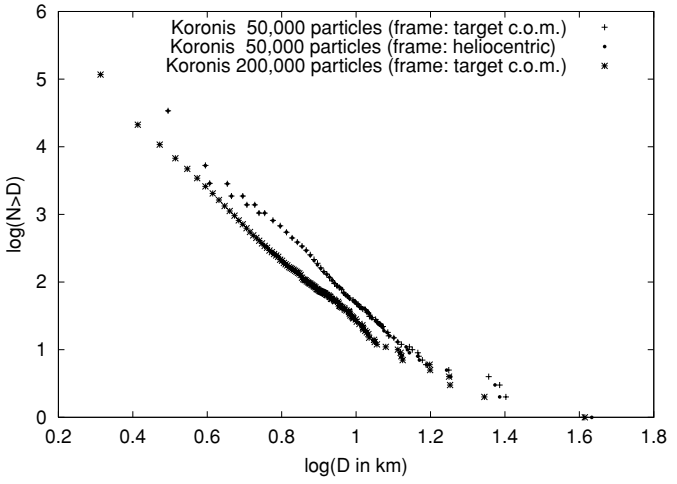

FIG. 4. Log–log plot of the cumulative diameter distributions (in km) of the fragments produced by the two simulations of the Koronis family with 5×10^4 particles and 2×10^5 particles. With the lowest resolution, one simulation was performed in the same frame as that of the simulation at higher resolution (i.e., target's center of mass isolated from any external perturbation), whereas the other was performed with the target placed 2.876 AU from the Sun. The two distributions with lower resolution were obtained 10.5 days after the impact. The one with higher resolution was obtained 23 days after the impact, which was necessary to reach the final M_{lr}/M_{pb} value.

becoming less steep (see Table II). Nevertheless, fragments of diameter greater than 10 km are produced similarly, showing that the possibility of bouncing does not have any major effects, even in high-energy regimes, on the formation of the largest fragments. However, the number of fragments produced by at least one reaccumulation is about 3 times smaller with SPIC than with STIC. This is simply due to the more frequent high-speed collisions between fragments in the catastrophic regime. Also, the difference in the distribution of ejection velocities is slightly greater for the two simulations than it was in lower-energy impact energy regimes (see Fig. 5 and Table II). Therefore, allowing for particle bouncing during the gravitational phase seems to be more important in the catastrophic regime, whereas it did not have any significant consequences in low- to intermediate-impact energy regimes.

Finally, in order to show that the chosen impact conditions are not unique and that other combinations can result in a statistically similar outcome, we simulated the break-up of the Koronis' parent body with two additional impact conditions. As we did for Flora (see Section 5), our aim was to reproduce a ratio M_{lr}/M_{pb} of the same order as the real one without looking for a good fit of the ejection velocity of the largest remnant. The two new impact conditions consider a projectile 20 km in radius impacting at (i) 3 km/s head on ($Q = 1.71 \times 10^9$ erg/g), and (ii) 4 km/s with an angle of incidence of 42 degrees ($Q = 3.04 \times 10^9$ erg/g). With perfect merging (STIC), the first impact condition leads to $M_{lr}/M_{pb} = 0.06$ and the second one gives $M_{lr}/M_{pb} = 0.057$. Both ratios are thus of the same order as the

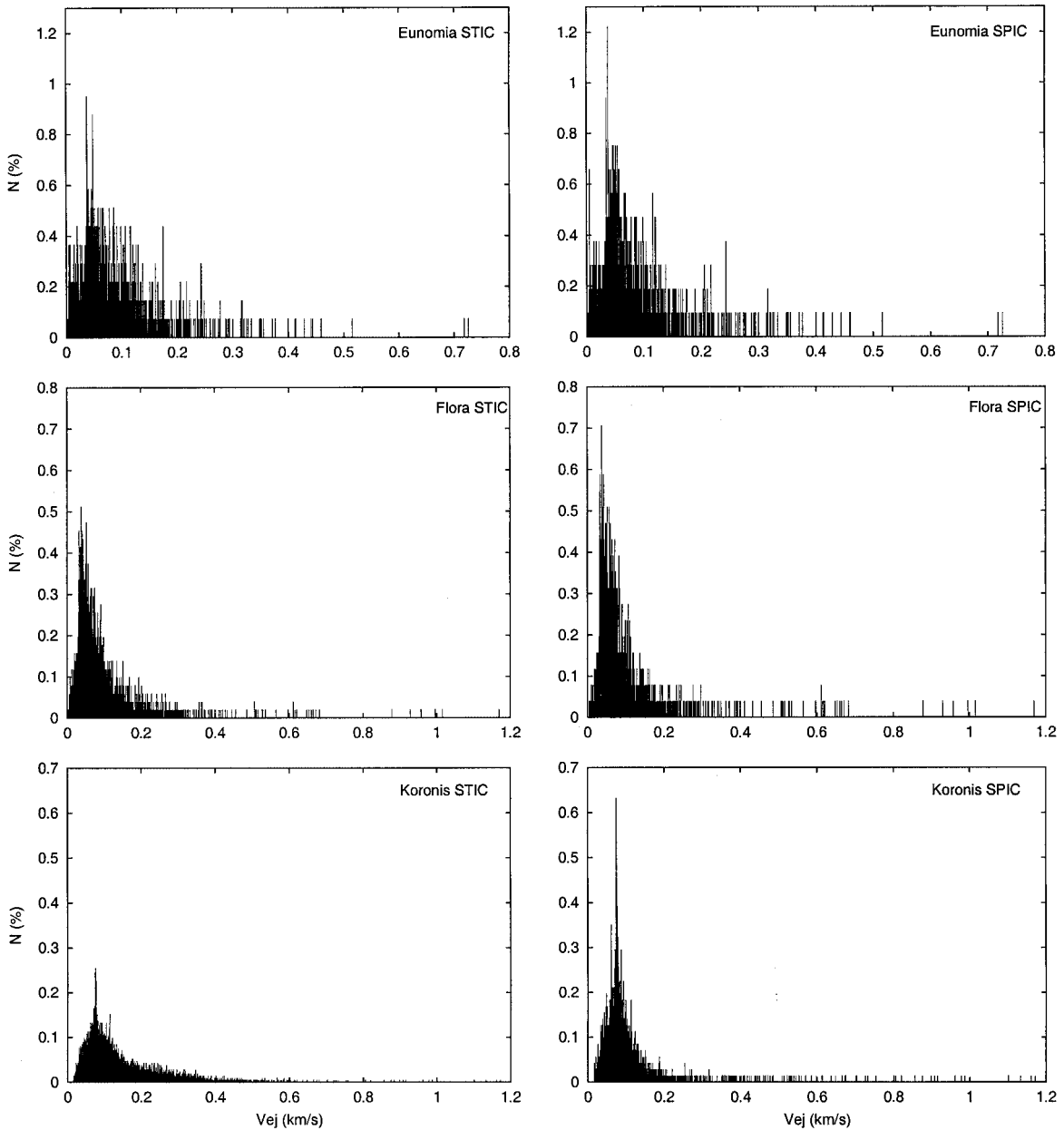

FIG. 5. Histogram of ejection velocities of fragments with size greater than the resolution for the three simulations of family formation. Left: simulations with perfect merging of colliding particles in the gravitational phase (STIC); right: simulations with particle bouncing allowed (SPIC). As in Fig. 1, the names at the top of the plots correspond to the real family names.

real ratio $M_{lr}/M_{pb} = 0.04$. Figure 6 shows that the slopes of the fragment size distributions are similar to each other and to the original STIC run. Only some minor differences are present for the largest fragment sizes. Thus, several impact conditions can lead to similar M_{lr}/M_{pb} ratios and statistically identical outcome properties. Note that for expediency we generated only two new impact conditions, but in each regime there is certainly a wide range of impact parameters that should lead to statistically similar outcomes.

5. IMPLICATIONS FOR THE PROPERTIES OF REAL FAMILIES

Several implications can be drawn from our simulations by comparing them in more detail with the observed properties of real families. Until recently, the common belief was that present asteroid families are simple images of their primordial structure. In fact, our current understanding of collisional and dynamical evolution instead indicates that the original properties of asteroid

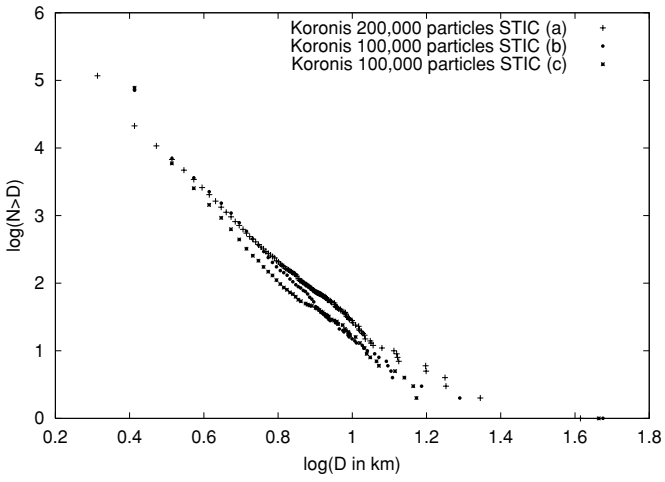

FIG. 6. Cumulative diameter distributions (in km) of the fragments resulting from the three simulations (STIC) of the Koronis family formation in a log–log plot. Three different projectile properties were used (in the following, $R_{\rm proj}$ is the projectile's radius, $V_{\rm proj}$ is the projectile's velocity, and θ is the angle of incidence): (a) $R_{\rm proj} = 30$ km, $V_{\rm proj} = 3.25$ km/s, $\theta = 75°$; (b) $R_{\rm proj} = 20$ km, $V_{\rm proj} = 3.00$ km/s, $\theta = 0°$; (c) $R_{\rm proj} = 20$ km, $V_{\rm proj} = 4.00$ km/s, $\theta = 42°$.

families are difficult to characterize since they depend on the subsequent collisional evolution of family members and on their complete orbital evolution. These effects are indeed not included in the secular perturbation theory used to derive their proper orbital elements. In particular, over time scales longer than a few 10^6 year, proper elements can significantly change, reflecting the accumulation of tiny nonperiodic effects caused by chaos and nonconservative forces. Therefore, though family identifications have been enabled and improved thanks to the development of sophisticated tools (Zappalà *et al.* 1995), the slope of their size distributions as well as the orbital dispersion of their members may well have been modified from their original values (see below for more detail). Thus, we cannot expect a perfect agreement between our simulations and the observed properties of these already evolved families. On the other hand, a comparison is important to check whether our results are consistent with studies on collisional and dynamical evolution of family members.

To compare the resulting size distributions of our simulations to those derived for the real families by Tanga *et al.* (1999), we have computed the powerlaw slope of the cumulative size distributions. Table II summarizes the results. It is important to recall that the size distributions of the real families are not directly observed but rather deduced from observations. For example, the albedo value used to convert magnitude into diameter is measured for only a few members, and below the completeness diameter, it is obtained from a geometric model (see Tanga *et al.* 1999 for details). In the case of Eunomia, the distribution of the real family was thus fit using a power-law exponent equal to -4.40 ± 0.42 (Tanga *et al.* 1999). Our STIC and SPIC simulations both result in a power-law exponent of -4.90 ± 0.16. For Flora, the real family is fit with a power-law exponent equal to -2.85 ± 0.17, whereas the fitting exponents of our STIC and SPIC simulations at 5.8 days after the impact are, respectively, -6.63 ± 0.21 and -5.58 ± 0.16. The fit at the same instant for the second STIC simulation resulting in a largest remnant with a smaller ejection velocity (14 m/s) gives an exponent of -7.99 ± 0.25. Finally, for the Koronis family, the power-law exponent fitting the real distribution is equal to -2.55 ± 0.34, whereas the ones found for our STIC and SPIC simulations with highest resolution (2×10^5 particles) are equal to, respectively, -4.56 ± 0.02 and -3.20 ± 0.02.

Generally, the size distributions obtained by SPIC are less steep than the ones by STIC, but they remain steeper than those of real families, which is consistent with subsequent collisional erosion. Indeed, studies of collisional evolution (see, e.g., Marzari *et al.* 1999) suggest that the subsequent collisional evolution of members of any given family leads progressively to a size distribution that converges toward a -2.5 power-law exponent (Dohnanyi 1971), starting from a greater absolute value. Interpreting the differences in slopes between the computed and observed families as a consequence of subsequent evolution indicates a young age for the Eunomia family, given the small difference in the slopes and assuming standard collisional erosion. Conversely for Koronis, an originally steeper slope is consistent with the estimated $\approx$1.5 billion-year age of the Koronis family, based on crater counts of member Ida's surface from Galileo spacecraft observations (Chapman *et al.* 1996). For Flora, the much steeper slopes from our simulations with respect to the one deduced from observations suggest that either (i) Flora was created a fairly long time ago, or (ii) the real family is poorly identified and its properties are not reliable. Scenario (i) seems improbable since recent studies have shown Flora lies in a region where many efficient diffusion mechanisms occur so that an old family would have already been evaporated. Possibility (ii) seems much more likely, as suggested by the spreading of real family members in proper element space (Fig. 7). This is also the reason why the Flora family is often called a *clan* rather than a family. In addition, and even worse for a reliable comparison, more than one family could actually coexist in this region. If this is the case, the outcome properties of a single break-up by even more realistic simulations may never be able to explain the observed properties. Thus, our simulations may in fact just provide some information on the break-up of a 164-km-size body in the intermediate regime, without a possibility to link it with a real case.

As we have just discussed, an important comparison concerns also the orbital dispersion of the fragments as a result of the break-up. Some results have already been published by Michel *et al.* (2001) concerning Eunomia and Koronis, showing that their current orbital dispersion is larger than the one resulting from the break-up itself. Recall that fragment orbital elements can be computed by Gauss formulae, which relate fragment velocities to orbital elements by giving for each member the distance of its orbital elements δa, δe, and δI to the barycenter of the family. The barycenter of Eunomia (i), Koronis (ii) and Flora (iii) are placed at: (i) $a_b = 2.643$ AU, $e_b = 0.148$ and

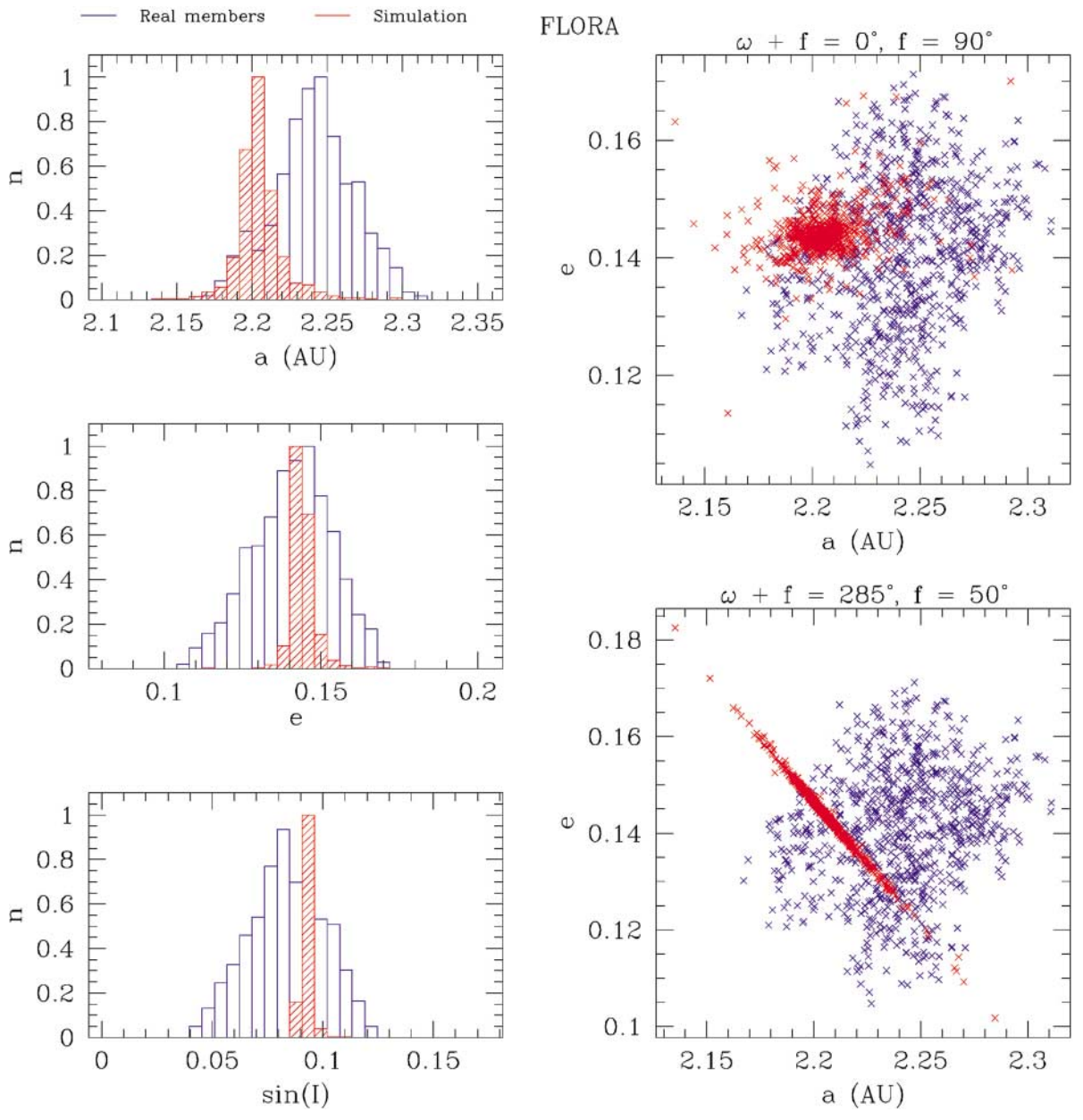

FIG. 7. Left: from top to bottom, histograms of the proper semi-major axis, eccentricity, and sine of inclination of both the real members of the Flora family (blue, open) and the simulated (STIC) family (red, filled). For the latter, the orbital elements are computed from Gauss' equations, assuming a main belt-like orbit of the projectile (see text for details). The values of the parent body's true anomaly at impact f and its sum with the argument of perihelion $\omega + f$ are assumed to be equal to, respectively, 90° and 0°. The histograms are individually normalized to the number of objects in the most populated bin. Right: distributions in the eccentricity versus semi-major axis plane of the real members (blue) and of the simulated (STIC) family (red) for two different values of f and $\omega + f$ of the parent body (indicated at the top of each panel), but for the same orbital parameters of the projectile. This shows the dependency of the shape in the (a, e) plane of the family of fragments immediately after the break-up on the chosen values of the unknown parent body's orbital angles.

$I_b = 13.1°$; (ii) $a_b = 2.866$ AU, $e_b = 0.048$ and $I_b = 2.1°$; and (iii) $a_b = 2.205$ AU, $e_b = 0.144$ and $I_b = 5.2°$. Gauss formulae up to the first order in eccentricity are then given by

$$\frac{\delta a}{a_b} = \frac{2}{n a_b \sqrt{1-e_b^2}}[(1+e_b\cos f)V_T + e_b \sin f V_R],$$

$$\begin{aligned} \delta e &= \frac{\sqrt{1-e_b^2}}{n a_b}\left[\frac{e_b + 2\cos f + e_b\cos^2 f}{1+e_b\cos f}V_T + \sin f V_R\right], \\ \delta I &= \frac{\sqrt{1-e_b^2}}{n a_b}\frac{\cos(\omega+f)}{1+e_b\cos f}V_W, \end{aligned} \quad (1)$$

where V_T, V_R, and V_W are the components of the ejection velocity

in the along-track, radial, and out-of-plane directions, respectively; n is the mean motion; f is the true anomaly of the parent body at the instant of the break-up; and ω is its argument of perihelion. These last two angles are not known, the most sensitive one being f (Zappalà *et al.* 1996). Assuming different values for this angle changes the shape and orientation of the cluster containing the family members in orbital element space, as Fig. 7 shows (see also Fig. 3 in Michel *et al.* 2001). Note also that the ejection velocities of our fragments are defined in the target's barycenter reference frame, with the z-axis in the direction of the projectile's impact velocity. In reality this orientation of the projectile is highly improbable. To be more realistic, we have considered main belt values as the orbital elements of the projectiles and used Öpik's theory (Öpik 1951) to derive from these values the direction of the impactor's velocity vector. Indeed, the impact velocity of the projectiles fixes the so-called Tisserand parameter,[1] which in turns fixes the projectile's eccentricity, given the values of the semi-major axis and inclination of the projectile, and the value of the semi-major axis of the parent body. The direction of the impactor's velocity vector can then be determined using Öpik's geometry, which then allows us to transform the components of the ejection velocities from the original reference frame to their components in the radial/along-track/out-of plane reference frame.

Concerning Koronis, Bottke *et al.* (2001) have confirmed that the observed properties do not represent the original positions of proper elements of the fragments following the break-up. In fact, they can be explained starting from the smaller dispersion produced by our simulations and letting the members evolve under the effects of slow diffusion mechanisms and nongravitational forces. In particular, high-order secular resonances, mean-motion resonances even involving two planets (Morbidelli and Nesvorný 1999), and the Yarkovsky thermal effect (Farinella and Vokrouhlický 1999) have recently been shown to be capable of altering the reliability of the proper element computation. While proper elements are conventionally assumed to retain memory of the initial positions, these recent studies have definitely demonstrated that this is not necessarily true, even for the proper semi-major axis when the asteroid is not too large. The current proper elements of family members can then hardly be interpreted as their original positions but are rather a result of such processes, whose effects are to diffuse family members in orbital element space, starting from a smaller dispersion. Thus, the degree of spreading observed now, together with the knowledge of the degree of dispersion resulting directly from the break-up, should better constrain the age of the family, once the efficiency of these diffusion processes is well known. As one can see, our simulations, which produce a denser grouping of the fragments than for the observed ones, are thus consistent with these studies on diffusion processes.

In the particular case of Flora, the denser grouping compared to the dispersion of real family members (Fig. 7) can also be interpreted as another argument for efficient diffusion in the Flora region. The values of the semi-major axis, eccentricity, and inclination of the projectile arbitrarily used to compute the distributions of the simulated families (Fig. 7) are equal to, respectively, 2.3 AU, 0.246, and 1.5°. Although we did not investigate the dependency of the shape of the family in the (a, e, $\sin(I)$) space on the full range of possible impactor orbital elements, several impactor orbital elements were tried and showed only slight differences in the grouping of the fragments in the (a, e) plane. Although this will have to be confirmed by a full investigation, this suggests that the critical parameters for the shape of the grouping are the true anomaly and argument of perihelion of the parent body at the instant of impact. Note also that both STIC and SPIC result in a similar degree of dispersion.

Dynamical studies of the Flora region have shown that many efficient diffusion mechanisms can occur, such as active mean-motion resonances with Mars and Jupiter (Nesvorný *et al.* 2002). Interestingly, Fig. 7 shows that the distribution of semi-major axes of our simulated families is off set on the left with respect to that of the real members. Such an offset requires that the real family members moved toward larger semi-major axes during their evolution. Actually, this supports a scenario proposed by Nesvorný *et al.* (2002). In this scenario, the parent body of the Flora family would have been disrupted at 2.2–2.23 AU, generating a tight grouping like the one produced in our simulation. The small fragments would then have drifted quickly toward smaller semi-major axes, due to the Yarkovsky effect, and would have been removed by the resonances and Mars encounters, while those drifting to larger semi-major axes could survive. Thus, the family would now appear more populated at larger semi-major axes than at its original position. Alternatively, the possible coexistence of more than one family identified as a wide single one is also not ruled out by our simulations and by Nesvorný *et al.* (2002). Therefore, it is still not possible to definitely conclude on the origin and characterization of the Flora family. Nevertheless, our simulations of the break-up of a Flora-like parent body in the corresponding regime provide at least some properties of a possible outcome of such an event.

[1] Strictly speaking, the Tisserand parameter is a constant in the restricted circular three-body problem but it is often used in the context of the close approach of a small body to a planet or a larger body. During such an encounter, as a first approximation, the system has the configuration of a three-body problem in which the Sun and the larger body are considered to be the main perturbers. In our problem, the larger body is the family's parent body and the Tisserand parameter is then $T = a_{pb}/a + 2\sqrt{a(1-e^2)/a_{pb}}\cos(I)$, where a_{pb} is the parent body's semi-major axis and a, e, I are, respectively, the semi-major axis, eccentricity, and inclination of the projectile's orbit (see, e.g., Carusi *et al.* 1987). Since T relates directly to the encounter velocity U of the projectile with the parent body by the expression $U = \sqrt{3-T}$, knowing this velocity sets T. Then, assuming some reasonable values of the semi-major axis and inclination of the projectile's orbit such that it is located in the main belt, the Tisserand parameter sets its eccentricity. This procedure thus allows us to set the orbital parameters of the projectile and thus the direction of the impact velocity vector.

TABLE III
Number of Satellites of the Largest Remnant (Percentage of the Total Number of SPH Particles) at the End of the Simulations for the Three Families

Family	Nb total	Nb total $Q < R_H$	Nb $R > R_{\min}$	Nb $R > R_{\min}$ $Q < R_H$	M_{ls}/M_{prim}
Eunomia STIC	352 (0.355)	328 (0.331)	37 (0.037)	36 (0.036)	8.8×10^{-5}
Eunomia SPIC	373 (0.377)	347 (0.350)	34 (0.034)	33 (0.033)	8.8×10^{-5}
Flora STIC	63 (0.032)	61 (0.031)	9 (0.004)	9 (0.004)	6.2×10^{-5}
Flora SPIC	91 (0.046)	88 (0.044)	6 (0.003)	6 (0.003)	7.1×10^{-5}
Koronis I STIC	973 (0.491)	911 (0.460)	276 (0.139)	258 (0.130)	0.02
Koronis I SPIC	1447 (0.731)	1259 (0.636)	187 (0.094)	158 (0.080)	0.035
Koronis II STIC	170 (0.301)	165 (0.292)	52 (0.092)	51 (0.09)	0.02

Note. The third column indicates the total number of satellites (percentage of the total number of SPH particles) with orbits entirely inside the Hill's radius of their primary. Q is the maximum distance to the primary of the satellite along its orbit. In the columns with $R > R_{\min}$, only objects with radius greater than the minimum value $R_{\min}$ imposed by the resolution of our simulations have been considered. The last column gives the mass ratio of the largest satellite to the primary. The higher mass ratio in the case of Koronis can be explained by the already small value of largest remnant mass itself (4% of the parent body mass).

6. SATELLITE FORMATION DURING COLLISIONS

One last important phenomenon is the natural and frequent production of small satellites of some fragments during a collisional event. The possibility that reaccretion may produce asteroid satellites has already been suggested by Durda (1996) and Doressoundiram *et al.* (1997), and many two-body systems (binaries) have now been observed (Merline *et al.* 1999), like the one involving the Koronis member Ida and its little moon Dactyl (Chapman *et al.* 1995). Our simulations, both STIC and SPIC, confirm the production of numerous satellites of the largest fragment. However, due to the complexity and wealth of data on the process of satellite formation following such collisions, we postpone a detailed study of this phenomenon to a forthcoming paper.

As an illustration, we list in Table III the number of satellites of the largest remnant only for each of the families. As one can see, in all cases, SPIC gives a smaller number of satellites with radius above the resolution than STIC, but a greater number of satellites in total. This is due to the fact that the possibility of bouncing prevents some reaccumulation to occur, and thus increases the number of particles with size equal to the resolution. Hence, this adds a possibility to generate satellites. In any case, both STIC and SPIC result in a large number of satellites for each family.

7. CONCLUSION

This work has extended the work of Michel *et al.* (2001) by showing new simulations aimed at testing the sensitivity of the previous results and thus at checking their robustness. Moreover, we improved the simulations of the gravitational phase of the collision by allowing the possibility of bouncing when two particles collide under certain conditions. Then, the intermediate impact energy regime, which leads to a mass ratio of the largest remnant to the parent body around 0.5, has been investigated, represented by the break-up of the Flora family parent body.

Our general conclusion is that our simulations, accounting for both the fragmentation and the gravitational interaction of the fragments, confirm the production of both large and dispersed bodies as observed in asteroid families and the formation of satellites around some asteroids. These phenomena result from reaccumulation during the gravitational phase of the collision. The robustness of this process is confirmed, since it occurs independent of the chosen values for the free parameters and the degree of sophistication in our simulations. This is the reason why laboratory experiments on centimeter-sized targets have failed to explain the asteroid family paradox (forming both large and dispersed fragments), gravitational interactions of fragments being negligible at this scale.

The results of these simulations compared to the corresponding families as we observe them today show some differences. However, the differences are fully consistent with our current understanding of the dynamical and collisional evolution of families, which indicate that (i) collisional erosion tends to reduce the slope of the fragments' size distribution and (ii) dynamical diffusion processes (resonances, Yarkovsky effect) spread their positions in proper element space.

Allowing the fragments to bounce when they collide during the gravitational phase does not result in statistically different outcomes compared to the previous simulations in which fragments always merged upon collision. But the possibility of bouncing adds two additional free parameters, which are the two coefficients of restitution (tangential and normal) of the fragments' velocities, arbitrarily set to 0.5 in this work. The sensitivity of the outcome on the value of these coefficients will be the subject of one of our future investigations. Also, we leave a detailed investigation of the fragment spin statistics in our

simulations to a separate study. A preliminary analysis suggests that the average spin values that we obtain are compatible with observations, independent of the impact energy regime.

Finally, we note that prior to a dispersing event, it is likely that bodies of sizes as large as family parent bodies have already been shattered by numerous previous small impacts, so that using a monolithic target may not appear realistic. A detailed analysis of rubble pile break-ups will be addressed in a forthcoming paper. We stress however that before being dispersed our parent bodies are also totally shattered during the fragmentation phase, and because gravity dominates over mechanical strength at these scales, this happens at correspondingly low energy costs. Consequently, while the collisional outcome may change in details, the internal structure of the parent bodies can certainly not prevent reaccumulation to occur.

Further analysis of family formation and more generally of collisional break-ups will also be done by applying our procedure in the future. Among the goals, one will be to study the different collisional regimes that can eventually lead to the injection of small bodies in transport routes to the Earth. According to our simulations, depending on its size, such a threatening body could be the result of gravitational reaccumulation, making it more resistant to impacts compared to a monolithic body (Asphaug *et al.* 1998). A good understanding of the collisional process and its possible outcomes is thus also required in the context of protection against potential Earth impactors.

ACKNOWLEDGMENTS

P.M. acknowledges financial support from the Action Thématique Innovante 2001 of the french Institut National des Sciences de l'Univers. W.B. acknowledges support from the Swiss National Science Foundation. P.T. has worked on this project while staying for two years at the Observatoire de la Côte d'Azur (O.C.A., France) thanks to the Henri Poincaré Fellowship. We are grateful to the ILGA team of the O.C.A. who generously provided access to their 4-processor COMPAQ DEC ALPHA workstation. Simulations were also partly carried out on the *SIVAM project* 4-processor COMPAQ DEC ALPHA of O.C.A. and on a Beowulf installed by the society *alineos* and partially financed by both the O.C.A. program *Bonus-Qualité-Recherches 2001* and the Cassini laboratory (O.C.A.). We also thank T. Quinn (U. Washington) for his fruitful advice on computational problems, Z. Leinhardt (U. Maryland) for comments, and A. Morbidelli, D. Durda and D. Vokrouhlický for their reviews and suggestions.

REFERENCES

Asphaug, E., and H. J. Melosh 1993. The Stickney impact of PHOBOS: A dynamical model. *Icarus* **101**, 144–164.

Asphaug, E., S. J. Ostro, R. S. Hudson, D. J. Scheeres, and W. Benz 1998. Disruption of kilometer-sized asteroids by energetic collisions. *Nature* **393**, 437–440.

Belton, B., C. R. Chapman, P. Thomas, M. Davies, R. Greenberg, K. Klaasen, D. Byrnes, L. D'Amario, S. Synnott, W. Merline, J. M. Petit, A. Storrs, and B. Zellner 1995. The bulk density of Asteroid 243 Ida from Dactyl's orbit. *Nature* **374**, 785–788.

Benz, W., and E. Asphaug 1995. Simulations of brittle solids using smooth particle hydrodynamics. *Comput. Phys. Comm.* **87**, 253–265.

Benz, W., and E. Asphaug 1999. Catastrophic disruptions revisited. *Icarus* **142**, 5–20.

Bottke, W. F., M. C. Nolan, R. Greenberg, and R. A. Kolvoord 1994. Velocity distributions among colliding asteroids. *Icarus* **107**, 255–268.

Bottke, W. F., D. Vokrouhlický, M. Brož, D. Nesvorný, and A. Morbidelli 2001. Dynamical spreading of asteroid families via the Yarkovsky effect. *Science* **294**, 1693–1696.

Carusi, A., Ľ. Kresák, E. Perozzi, and G. B. Valsecchi 1987. High-order librations of Halley-type Comets. *Astron. Astrophys.* **187**, 899–905.

Cellino, A., P. Michel, P. Tanga, V. Zappalà, P. Paolicchi, and A. Dell'Oro 1999. The velocity-size relationship for members of asteroid families and implications for the physics of catastrophic collisions. *Icarus* **141**, 79–95.

Chapman, C. R., D. R. Davis, and R. Greenberg 1982. Apollo asteroids: Relationships to main belt asteroids and meteorites. *Meteoritics* **17**, 193–194.

Chapman, C. R., P. Paolicchi, V. Zappalà, R. P. Binzel, and J. F. Bell 1989. Asteroid families: Physical properties and evolution. In *Asteroids II* (R. P. Binzel, T. Gehrels, and M. S. Matthews, Eds.), pp. 386–415. Univ. of Arizona Press, Tucson.

Chapman, C. R., J. Veverka, P. C. Thomas, K. Klaasen, M. J. S. Belton, A. Harch, A. McEwen, T. V. Johnson, P. Helfenstein, M. E. Davies, W. J. Merline, and T. Denk 1995. Discovery and physical properties of Dactyl a satellite of Asteroid 243 Ida. *Nature* **374**, 783–785.

Chapman, C. R., E. V. Ryan, W. J. Merline, G. Neukum, R. Wagner, P. C. Thomas, J. Veverka, and R. J. Sullivan 1996. Cratering on Ida. *Icarus* **120**, 77–86.

Davis, D. R., C. R. Chapman, S. J. Weidenschilling, and R. Greenberg 1985. Collisional history of asteroids: Evidence from Vesta and the Hirayama families. *Icarus* **62**, 30–53.

Dohnanyi, J. S. 1971. Fragmentation and distribution of asteroids. In *Physical Studies of Minor Planets* (T. Gehrels, Ed.), pp. 263–296. NASA SP-267, Washington DC.

Doressoundiram, A., P. Paolicchi, A. Verlicchi, and A. Cellino 1997. The formation of binary asteroids as outcomes of catastrophic collisions. *Planet. Space Sci.* **45**, 757–770.

Durda, D. D. 1996. The formation of asteroidal satellites in catastrophic collisions *Icarus* **120**, 212–219.

Farinella, P., and D. R. Davis 1992. Collision rates and impact velocities in the main asteroid belt. *Icarus* **97**, 111–123.

Farinella, P., and D. Vokrouhlický 1999. Semimajor axis mobility of asteroidal fragments. *Science* **283**, 1507–1510.

Farinella, P., D. R. Davis, and F. Marzari 1996. Asteroid families, old and young. In *Completing the Inventory of the Solar System* (T. W. Rettig and J. M. Hahn, Eds.), ASP Conference Series 107, pp. 45–55. ASP, San Francisco.

Jaeger, J. C., and N. G. W. Cook 1969. *Fundamentals of Rock Mechanics.* Chapman & Hall, London.

Lazzaro, D., T. Mothé-Diniz, J. M. Carvano, C. A. Angeli, and A. S. Betzler 2001. The Eunomia family: A visible spectroscopic survey. *Icarus* **142**, 445–453.

Marzari, F., D. Davis, and V. Vanzani 1995. Collisional evolution of asteroid families. *Icarus* **113**, 168–187.

Marzari, F., P. Farinella, and D. R. Davis 1999. Origin, aging, and death of asteroid families. *Icarus* **142**, 63–77.

Merline, W. J., L. M. Close, C. Dumas, C. R. Chapman, F. Roddier, F. Menard, D. C. Slater, G. Duvert, C. Shelton, and T. Morgan 1999. Discovery of a moon orbiting the Asteroid 45 Eugenia. *Nature* **401**, 565–568.

Michel, P., W. Benz, P. Tanga, and D. C. Richardson 2001. Collisions and gravitational reaccumulation: Forming asteroid families and satellites. *Science* **294**, 1696–1700.

Migliorini, F., V. Zappalà, and A. Cellino 1995. Interlopers within asteroid families. *Icarus* **118**, 271–291.

Milani, A., and Z. Knežević 1990. Secular perturbation theory and computation of asteroid proper elements. *Celest. Mech.* **49**, 347–411.

Milani, A., and Z. Knežević 1992. Asteroid proper elements and secular resonances. *Icarus* **98**, 211–232.

Milani, A., and Z. Knežević 1994. Asteroid proper elements and the dynamical structure of the asteroid belt. *Icarus* **107**, 219–254.

Morbidelli, A., and D. Nesvorný 1999. Numerous weak resonances drive asteroids toward terrestrial planets orbits. *Icarus* **139**, 295–308.

Murray, N., and M. Holman 1997. Diffusive chaos in the outer asteroid belt. *Astron. J.* **114**, 1246–1259.

Nesvorný, D., A. Morbidelli, D. Vokrouhlický, W. F. Bottke, and M. Brož 2002. The Flora family: A case of the dynamically dispersed collisional swarm? *Icarus* **157**, 155–172.

Öpik, E. J. 1951. Collision probabilities with the planets and the distribution of interplanetary matter. *Proc. R. Irish. Acad.* **54**, 165–199.

Pravec, P., and A. W. Harris 2000. Fast and slow rotation of asteroids. *Icarus* **148**, 12–20.

Richardson, D. C. 1994. Tree code simulations of planetary rings. *Mon. Nat. R. Astron. Soc.* **269**, 493–511.

Richardson, D. C., T. Quinn, J. Stadel, and G. Lake 2000. Direct large-scale N-body simulations of planetesimal dynamics. *Icarus* **143**, 45–59.

Richardson, D. C., Z. M. Leinhardt, W. F. Bottke, Jr., H. J. Melosh, and E. Asphaug 2002. Gravitational aggregates: Evidence and evolution. In *Asteroids III* (W. F. Bottke, Jr., A. Cellino, P. Paolicchi, and R. P. Binzel, Eds.), in press. Univ. of Arizona Press, Tucson.

Ryan, E. V., and H. J. Melosh 1998. Impact fragmentation: From the laboratory to asteroids. *Icarus* **133**, 1–24.

Tanga, P., A. Cellino, P. Michel, V. Zappalà, P. Paolicchi, and A. Dell'Oro 1999. On the size distribution of asteroid families: The role of geometry. *Icarus* **141**, 65–78.

Thomas, P. C., J. Joseph, B. Carcich, B. E. Clark, J. Veverka, J. K. Miller, W. Owen, B. Williams, and M. Robinson 2000. The shape of Eros from NEAR imaging data. *Icarus* **145**, 348–350.

Tillotson, J. H. 1962. *Metallic Equations of State for Hypervelocity Impact.* General Atomic Report GA-3216, July 1962.

Weibull, W. A. 1939. A statistical theory of the strength of material (transl.). *Ingvetensk. Akad. Handl.* **151**, 5–45.

Yeomans, D. K., and 12 colleagues 1997. Estimating the mass of Asteroid 253 Mathilde from tracking data during the NEAR flyby. *Science* **278**, 2106–2109.

Zappalà, V., P. Bendjoya, A. Cellino, P. Farinella, and C. Froeschlé 1995. Asteroid families: Search of a 12,487-asteroid sample using two different clustering techniques. *Icarus* **116**, 291–314.

Zappalà, V., A. Cellino, A. Dell'Oro, F. Migliorini, and P. Paolicchi 1996. Reconstructing the original ejection velocity fields of asteroid families. *Icarus* **124**, 156–180.